International Journal of Material Forming (2024) 17:54
https://doi.org/10.1007/s12289-024-01853-9

ORIGINAL RESEARCH

Electromagnetic blank holding system for flexible segmentation in forming of complex parts: a flow rate-based design, configuration, and validation

Lei Li[1,2,3] · Mengxiao Yang[1,2] · Yue Wang[4] · Lei Gan[1,2] · Haihong Huang[1,2]

Received: 13 March 2024 / Accepted: 27 August 2024

Abstract
Using a segmented holding system can effectively reduce cracking and wrinkling in the stamping process and improve the forming limit of stamped parts. Different segmentation schemes can be achieved flexibly using a blank holding system driven by electromagnetics. However, how to segment the blank holder to fulfill the demand for flow control of complex parts is still an obstacle to overcome. This paper proposes a flow rate-based design of distributed blank holders on demand for complex parts. A theoretical model is first established to analyze the differences in flow rate in the flange. Then, the flow rates are identified circumferentially and radially to find the locations where the changes in rates are large, and these locations are lined and deemed as the boundaries for segmenting holders. Moreover, a design implementation, including location identification and the electromagnetic system configuration for complex parts, is developed to explore the optimal segmentation schemes. To validate the effectiveness, the downscaling part of a car door with the material DP600 is selected to find the segmented scheme, and the corresponding prototypes of integral and segmented electromagnetic dies are then configured. Experimental results show that the thickening ratio is decreased by 15.4%, and the thinning ratio is increased by 22.5% compared with that of the integral blank holder, and the design achieves better quality and fewer segmented pieces compared with the conventional approach. This research assists in designing segmented blank holding systems enabled by electromagnetics and provides a universal segmentation approach to form better-quality complex parts.

Keywords Segmented blank holder · Flow rate · Complex part · Electromagnetic holding

Introduction

Parts with complex geometries are widely used in automobiles [1], aviation, and other fields. In the automotive field, the weight of stamped parts, which accounts for about 1/4 to 1/3 of the total weight of the body, ranks first among the various parts. With the increased complexity of the parts, the stamping process [2] faces new challenges. For example, wrinkling and cracking are prone to occur during the stamping process. The material flow in a complex surface stamping process is closely related to the change of the loading position of the blank holding force with the stamping stroke [3]. To reduce defects, the problem of uneven blank flow at different locations must be alleviated or eliminated by segmented blank holders [4]. Conventional mechanical or hydraulic blank holders have limitations, such as complex structures and low flexibility. To overcome these disadvantages, a blank holding system driven by electromagnetics was proposed [5], and the control for high accuracy of the blank holding force was addressed [6]. With the help of electromagnetics, different segmented schemes can be achieved flexibly. However, segmenting the blank holder to fulfill the demand for flow control of complex parts is still an obstacle.

To fill the gap, an electromagnetic blank holding system suitable for segmentation to stamp complex parts is

✉ Haihong Huang
huanghaihong@hfut.edu.cn

1 School of Mechanical Engineering, Hefei University of Technology, Hefei 230009, P. R. China

2 Key Laboratory of Green Design and Manufacturing of Mechanical Industry, Hefei University of Technology, Hefei 230009, P. R. China

3 Intelligent Manufacturing Institute of Hefei University of Technology, Hefei 230051, P. R. China

4 Cummins Inc., 500 Jackson Street, Columbus, IN 47201, USA

Published online: 19 September 2024

proposed. The system considers the flow of a blank and a flow rate-based segmenting approach for distributed blank holders. The stress and strain of the flange in the blank in the stamping process are taken as the starting point, and the rates of the flange nodes at different depths in the stamping process are analyzed. Then, using the flow rate of the nodes in the flange as the reference quantity, the blank holder's circumferential and radial segmentation boundaries are identified. Finally, the blank holder is reasonably segmented into distributed sub-areas.

Literature review

Circumferential segmentation of the blank holders

The configuration of the segmented blank holder can be dated to over twenty years ago. Siegert et al. used hydraulically supported segmented binders to build a control system with special dies [7]. Previous research on blank holder segmentation mainly applies two approaches, i.e., circumferential and radial segmentations.

Li et al. showed that circumferentially segmented blank holders could effectively regulate the blank flow and strain distribution [8]. Tommerup et al. proposed an active tooling system capable of controlling the distribution of the blank holding force using four integrated hydraulic chambers for the individual control of the blank holding force [9]. Fallahiaarezoodar et al. achieved favorable aluminum alloy formability by employing a servo-hydraulic cushion device to accurately control the blank holding force during forming [10]. Modi et al. investigated the influence of process parameters on the formability of a component by utilizing a hydraulic system to provide stamping force and blank holding force [11]. Sritat et al. segmented the box-shaped part blank holder into straight edge and rounded corner areas to improve the blank forming quality [12]. Hassan et al. segmented the blank holder into upper and lower layers, raising the box stamping limit [13]. Kitayama et al. simultaneously optimized the circumferential blank holding force and blank shape of each block, and validated its effectiveness in the stamping process of box-shaped parts [14], and the team also adjusted the circumferential segmentation blank holder area, reducing the energy consumption of the process [15]. Liu et al. used a circumferential segment holder system for spherical parts, which resulted in a more uniform blank flow and improved the thickness uniformity of the formed parts [16].

When using the circumferential segment holder to deepen the formed part, the thickness of the flange blank varies significantly along the radial direction. The blank holder can only create an effective holding in thick areas, and the blank holder cannot form an effective holding in thin areas.

Radial segmentation of the blank holders

Circumferential segment holder results in the uneven flow rate of the blank in the radial direction. Segmenting the blank holder into blocks along the radial direction can solve the problem of uneven radial deformation of the blank thickness.

Tran et al. proposed a novel method of varying blank holding force using a segmented blank holder and investigated its influence on reducing earing in the circular deep drawing process of an aluminum alloy sheet [17]. Endelt et al. utilized a flexible blank holder system to independently adjust the blank holding force in different regions of the flange area [18]. Seo revealed the effectiveness of blank holder force control using an electromagnetic blank restrainer [19]. Qin et al. investigated the critical value of the crimping force along the radial direction in the flange zone of the barrel part to show the necessity of radial segmentation and improve the stamped part's forming effect [20]. Zhang et al. segmented the blank holder radially into two parts, which well suppressed the wrinkling of the blank and improved the forming limit [21], and demonstrated that the diameter of the radially segmented blank holder significantly influenced the forming effect [22]. Based on this, the team segmented the blank holder into multiple blank holders along the radial direction and found a more reasonable ratio of blank holding force distribution [23]. Kelin et al. simplified the model for flange wrinkling using the energy method, which involved updating the flange geometry and material hardening parameters to predict the occurrence of flange wrinkling [24].

These studies show that circumferentially or radially segmented blank holders can achieve uniform strain and stress, thus improving forming quality. However, the thickness difference between the flange's outer edge and the deformation mass's inner edge in the rounded corner area cannot be effectively avoided. So, research on the hybrid segmentation method combining circumferential and radial segmentation has been carried out to solve the problem. Qin et al. proposed a hybrid segmentation method, and the circumferential segmentation was first completed, and the radial segmentation was performed for the rounded corner area, then the team introduced the electro-permanent magnet technology to continue the study of hybrid segmentation crimping, which significantly improved the forming capability of the blank [25]. Endelt et al. addressed controlling the flange draw-in using a distributed blank-holder force and variable total blank-holder force [26].

All the studies above have improved the forming quality and forming limit by segmenting the blank holder reasonably and applying proper blank holding force. However, the forming

parts selected in these studies are all cylindrical and box-shaped pieces with a single feature, and the segmentation approaches of the blank holder are based on the geometry characteristics of the die and the thickness of the blank. For a part with complex geometries, it is still challenging to unify the deformation of the blank [27]. Therefore, an electromagnetic blank holding system for flexible segmentation in forming complex parts is proposed and configured to solve this problem.

The rest of this paper is organized as follows: the electromagnetic blank holding system for flexible segmentation and the flow rate-based segmented design based on the theoretical analysis are proposed in "Methodology" section. The configuration of the segmented electromagnetic holder for the downscaling part of a car door is designed based on the approach and is installed on the hydraulic press for better forming, and results are analyzed and discussed in "Results and discussions" section. Finally, conclusions were drawn in "Conclusions" section.

Methodology

Segmented blank holding system driven by electromagnetics

Based on our previous work in Ref. [5], an improved blank holding system driven by electromagnetics for flexible segmentation of holders is developed for better force transmission, as illustrated in Fig. 1(a). The main components of this electromagnetic segmentation holding system include the blank holder, the amplification plate, and the electromagnetics device that provides the BHF, i.e., blank holding force. The magnet, which can generate electromagnetic force when being energized, is installed in the die and can move together with the die. Each amplification plate, i.e., AMP, is connected to a segmented blank holder. The blank holder is distributed along the circumferential and radial directions and acts on the flange to apply BHF, i.e., AMP I for the straight side and AMP II for the corner in View A in Fig. 1(b). The amplification plate (AMP) is supported by a gas spring underneath, and the gas spring is mounted at the lower base with a clearance fit. When the device carrying the electromagnet is close to the blank, the magnet will be energized to attract the amplification plate, which will be subjected to an upward force that will drive the blank holder to clamp the blank (see View B in Fig. 1(b)), thus converting the electromagnetic force into BHF. The deformation of the blank will then occur with the downward movement of the die and the electromagnetic device.

The basic purpose of the electromagnetic holding system is to use electromagnetics to generate holding force acting on the flange, thus completing the stamping process, as shown in Fig. 1(c). The blank holding force in this system is derived from the attractive force of the magnet. The EPM comprises magnetic poles (MPs), coils, yokes, soft magnets, and permanent magnets. Each magnetic pole is surrounded by permanent magnets, and each soft magnet is surrounded by a multi-turn coil that provides a magnetizing (or demagnetizing) field. When the magnetization direction of the soft magnet, which is determined by the current direction of the coil, aligns with that of the permanent magnet, the electro-permanent magnet will attract the amplification plate, and the attractive force increases as the current increases, which is shown as the magnetization in Fig. 1(c). While the direction of the current is reversed, the direction of magnetization of soft magnets is opposite to that of the permanent magnets, and electromagnetic force can be reduced to near zero when the magnitude of the current is large enough, which is shown as demagnetization in Fig. 1(c).

With the amplification plate, the force can be transferred to each segmented holder quickly and flexibly. The following sections will address how to segment the holder for a better quality of the part with complex geometries.

Flow rate-based segmentation design

In drawing up parts with complex geometries, the flow rate of the flange varies due to different stresses. The differences in flow rate affect the forming quality of the stamping parts. Based on the flow rate of the flange blank, different blank holder forces are applied to different blank holders through the circumferentially and radially segmented holders. This approach will control and equalize the flow rate of the flange, and improve the forming quality of stamping parts. The flow rate-based segmentation design is illustrated, as shown in Fig. 2.

In this approach, the flow rate is obtained by analyzing the stress and strain in different flanges. On the circumferential base, due to the uneven flow of the blanks, stacking the blanks in the slowest section incurs wrinkles, causing only the larger thickness of the flange to contact the blank holder. Because of this, the circumferential blank holder is segmented radially for distributed holding, which solves the problem of uneven thickness. The approach's effectiveness is validated, and four forming quality metrics, i.e., maximum thickening ratio, maximum thinning ratio, average thickness, and equivalent plastic strain, are checked (see Table 8 in Appendix 1). With the segmented scheme of the holder, the holding system was designed by considering the area of each holder, the area of the AMP, etc., according to "Segmented blank holding system driven by electromagnetics" section.

To clearly state the flow rate identified in this study, it is defined as follows by taking the rounder corner as an example according to Refs [30 and [31], as shown in Fig. 3. In this figure, R_0 is the initial equivalent radius of the blank, the distance from the center of

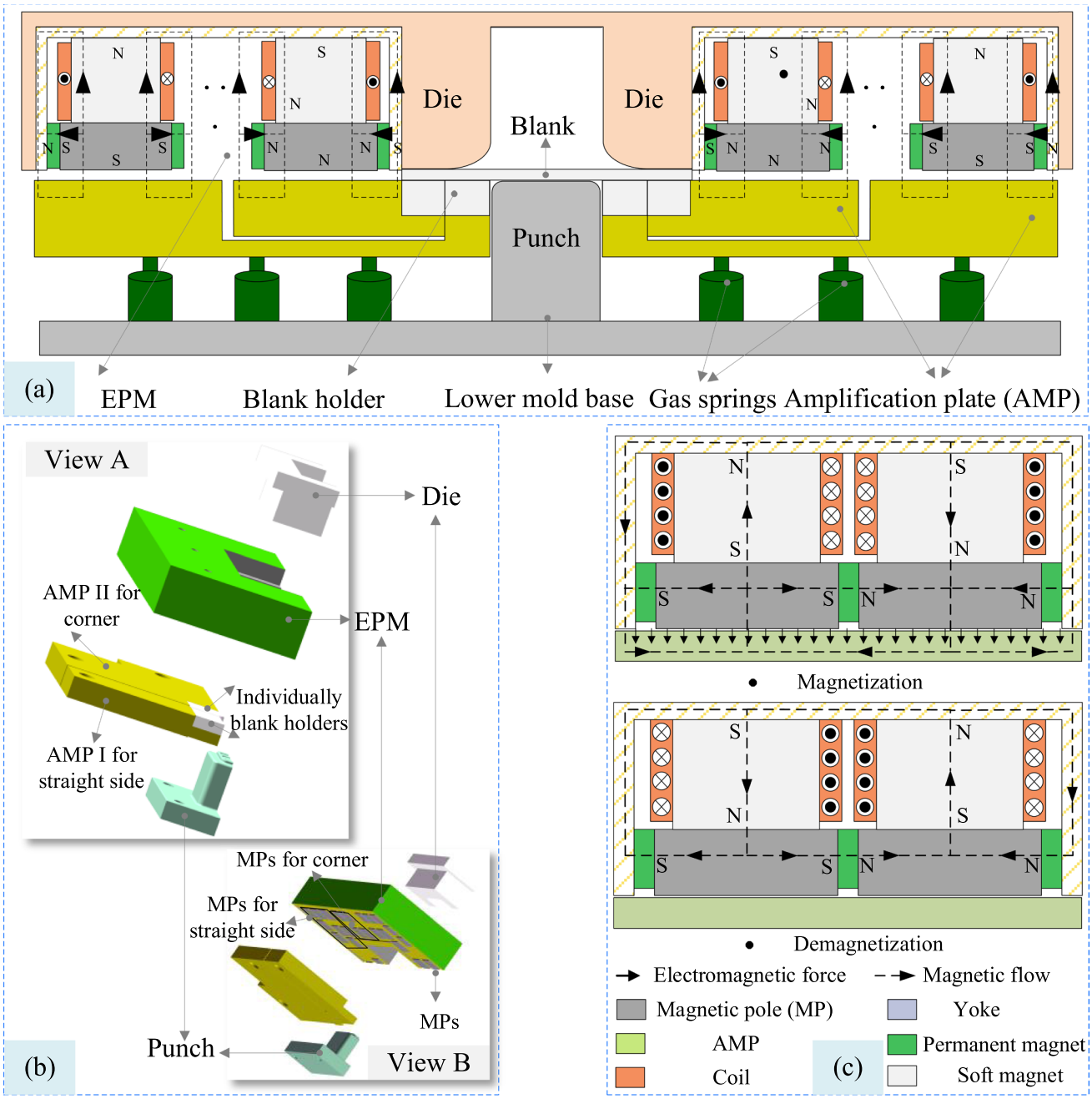

Fig. 1 Schematic diagram of the proposed blank holding system driven by electromagnetics.(**a**) Sectional view of the blank holding system, (**b**) Disassembly diagram of the EPM and holders, and (**c**) Magnetization and demagnetization for blank holding of the EPM. (The EPM indicates an electro-permanent magnet, AMP represents the amplification plate, and MP denotes the magnetic pole of the EPM)

the die fillet radius along the shear zero line to the outermost edge of a complex curved part, R is the radius of a particle at any position on the flange, R_W is the instantaneous equivalent radius of complex curved parts, i.e., the radius of the outer edge of the flange zone at any given moment, and r_0 is the die radius of the flange.

The flow rate of any point, i.e., $v_k(x_i, y_i)$, in the flange upward, can be expressed as

$$v_k(x_i, y_i) = \sqrt{v_r^2 + v_\theta^2} \tag{1}$$

Flow velocities in the radial and circumferential directions, i.e., v_r and v_θ, can be expressed as

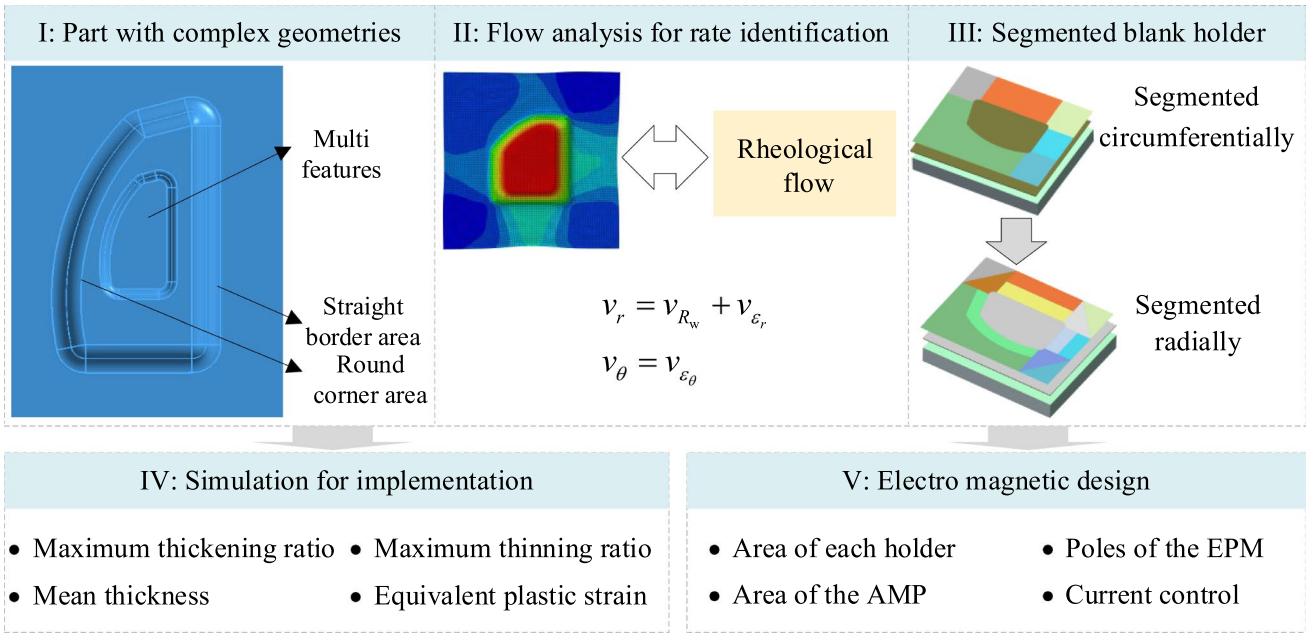

Fig. 2 Flow rate-based segmented approach for the part with complex geometries

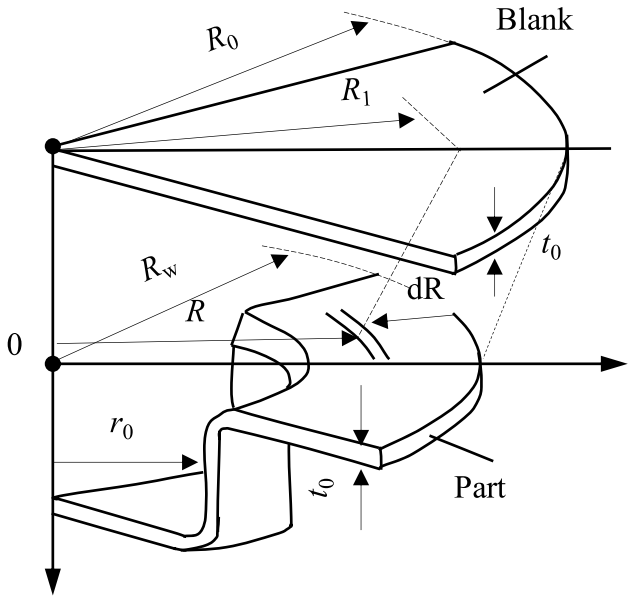

Fig. 3 Flow of the flange in the rounder corner during stamping

$$\begin{aligned} v_r &= v_{R_w} + v_{\varepsilon_r} = \frac{R}{R_0^2 - R_w^2 + R^2} - \frac{1}{R} - \frac{R_w}{r_0} v_0 \\ v_\theta &= v_{\varepsilon_\theta} = \frac{1}{R} - \frac{R}{R_0^2 - R_w^2 + R^2} \end{aligned} \tag{2}$$

The velocity of the edge, i.e., v_{R_w}, can be expressed as

$$v_{R_w} = \frac{dR_w}{dt} = -\frac{R_w}{r_0}\frac{dh}{dt} = -\frac{R_w}{r_0} v_0 \tag{3}$$

According to the principle of volume invariance, strain in the circumferential and radial directions, i.e., ε_θ and ε_r, can be respectively expressed as

$$\begin{aligned} \varepsilon_\theta &= \ln \frac{R}{\sqrt{R_0^2 - R_w^2 + R^2}} \\ \varepsilon_r &= -\ln \frac{R}{\sqrt{R_0^2 - R_w^2 + R^2}} \end{aligned} \tag{4}$$

Circumferential segmentation of a blank holder

For parts with complex geometries, the stress and strain vary in different locations in the flange. The adjacent areas of the blank will generate different deformations of radial elongation or circumferential compression. When the stamping stroke starts, the nodes $N(x_i,y_i)$ in the flange corresponding to the blank flow rate $v(x_i,y_i)$ are also different. To identify the flow rate and its change along the circumferential directions, nodes are set in the flange. The segmented approach of the blank holder along the circumferential direction based on the flow rate of nodes is illustrated in Fig. 4.

A closed-loop node set, i.e., $N_1(x_i,y_i)$ in line l_1, is first selected at the innermost relative equal radius distance of the flange. The closed-loop set is selected from the inside out, and other closed-loop node sets $N_k(x_i,y_i)$ in line l_k are selected similarly to ensure

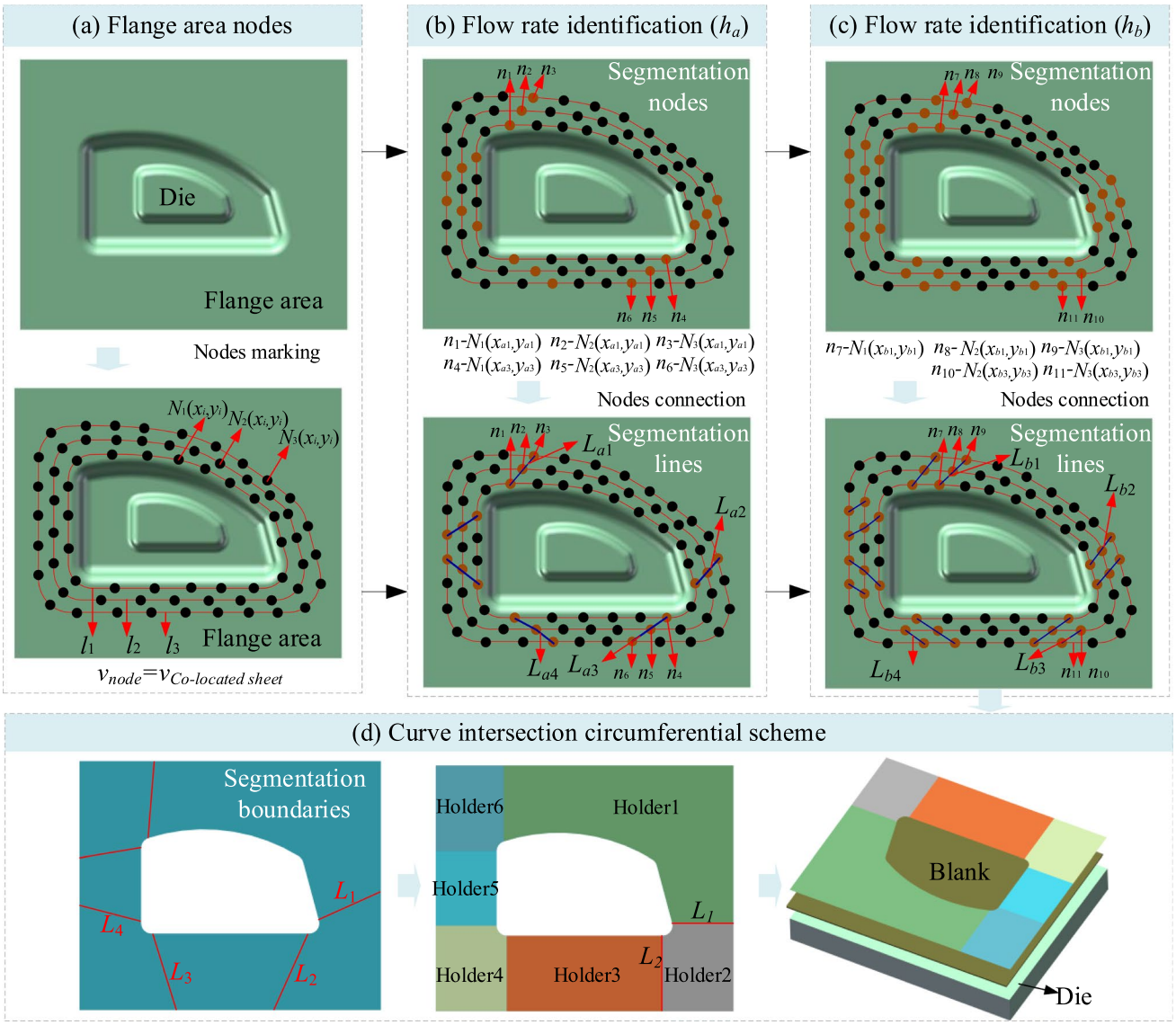

Fig. 4 Segmented circumferentially of blank holder based on the flow rate.(**a**) Nodes selected circumferentially on the flange, (**b**) Flow rate identification and line nodes with similar rates when the stamping depth reaches h_a, (**c**) Flow rate identification and line nodes with similar rates when the stamping depth reaches h_b, and (**d**) Curve intersection of the lines for circumferential segmentation

that the flange can be fully covered. Note that three closed-loop sets, i.e., l_1, l_2, and l_3, are marked in Fig. 4(a).

When the stamping reaches the depth of h_a, the rates at different nodes in a closed-loop node set are generated as a line graph. Due to the different stresses subjected to inevitably lead to abrupt changes or transitions in the rates of adjacent nodes, there will be a ratio of change between the rates of two adjacent nodes, which can be expressed as Eq. (5).

$$\left|\frac{v_k(x_{i+1},y_{i+1})-v_k(x_i,y_i)}{v_k(x_i,y_i)}\right| \geq q \tag{5}$$

where $v_k(x_i,y_i)$ is the rate of $N_k(x_i,y_i)$ node and q is the threshold ratio of change between adjacent nodes, which indicate the similarity of the flow rate in different areas, and the range is given as [25%, 30%].

When the ratio of change between two adjacent nodes is greater than q, $N_1(x_{a1},y_{a1})$, $N_2(x_{a1},y_{a1})$, and $N_3(x_{a1},y_{a1})$ can be determined as the circumferential segmentation nodes of the blank holder. The segmentation nodes in different closed loop sets in the same location area are connected as the circumferential segmentation line of the overall blank holder, i.e., L_{a1}, and the other three circumferential segmentation lines are also marked, i.e., L_{a2}, L_{a3}, and L_{a4}, as shown in Fig. 4(b).

When the stamping depth is h_b, the pressure on the sides and the stress on each blank section will change accordingly. The locations of the segmented circumferential nodes

also play a role. The circumferential segmentation line can be determined in the same way, i.e., $N_1(x_{b1},y_{b1})$, $N_2(x_{b1},y_{b1})$, and $N_3(x_{b1},y_{b1})$ in line L_{b1}, and the other three circumferential segmentation lines are identified as L_{b2}, L_{b3}, and L_{b4}, as shown in Fig. 4(c). The intersection lines can be used as the boundaries of circumferential segmentation. Figure 4(d) shows an example where L_1, L_2, L_3, and L_4 are the boundaries of the blank holder at different locations.

Segmentation of distributed blank holder based on flow rate

When the stroke begins, and the blank enters a depth, the radial force of the blank is different in the radial direction, and the flow rate at each flange node is also different. For different circumferential holding areas, nodes $M_1(x_i,y_i)$ in set w_1 from the innermost location to the outermost edge of each circumferential flange between L_1 and L_2, are selected at the geometric radial centerline of different blank holders. The number of nodes is set according to the demand to ensure comprehensive node data, and the value should ensure that sufficient radial node data are obtained at different depths. The other set, i.e., w_2, is also marked, as shown in Fig. 5(a).

When stamping to depth h_c, for the change ratio of the adjacent node rate greater than q, the segmentation node $M_1(x_{c1},y_{c1})$ can be considered as a radial segmentation node. The line perpendicular to the radial center line where the segmentation node is located, i.e., w_1, is deemed as the radial segmentation line of this circumferential blank holder, i.e., W_{c1}. The other radial

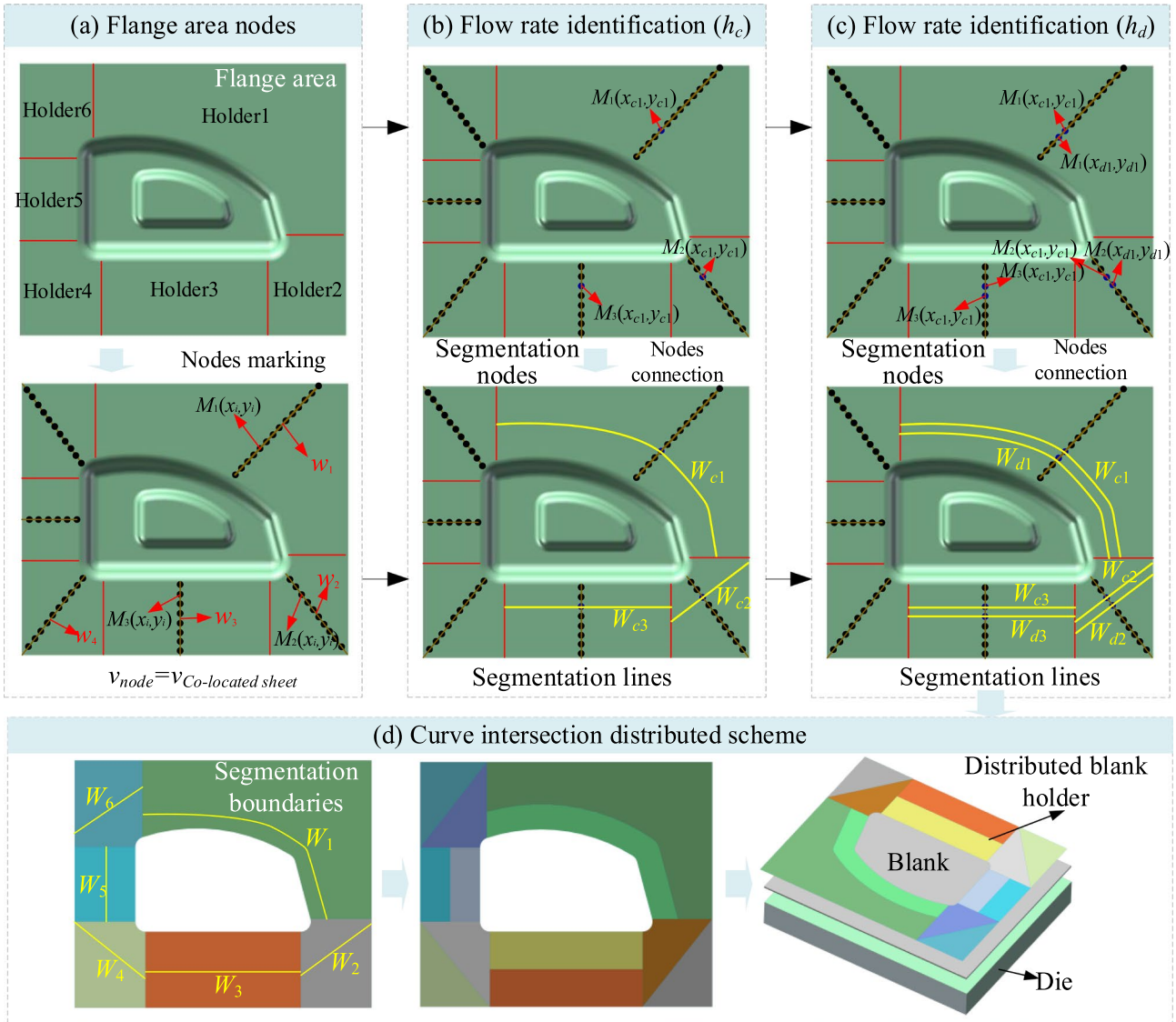

Fig. 5 Segmented radially of blank holder based on the circumferential flange node rate. (**a**) Nodes selected radially on the flange, (**b**) Flow rate identification and line nodes with similar rates when the stamping depth reaches h_c, (**c**) Flow rate identification and line nodes with similar rates when the stamping depth reaches h_d, and (**d**) Curve intersection of the lines for distributed segmentation

segmentation line, i.e., W_{c2} is also marked, as shown in Fig. 5(b). When depth increases to h_d, the compression force and the stress of each blank area will change accordingly. The radial segmentation nodes $M_1(x_{d1},y_{d1})$ and $M_2(x_{d1},y_{d1})$ and the corresponding radial segmentation lines, i.e., W_{d1} and W_{d2} in the circumferential area are determined accordingly, as shown in Fig. 5(c). This way, the segmentation nodes at each stamping depth and the segmentation boundaries are marked in the different circumferential holding areas until the stamping is finished. All the radial segmentation lines at different circumferential locations at the downstream depth can be determined, and the intersection line is deemed as the corresponding radially segmented boundary, i.e., W_1 and W_2, as shown in Fig. 5(d). Combining the above-mentioned radial and circumferential arrangement on the pressure side, the flow rate of the flange can be effectively controlled by the distributed scheme of holders.

Implementation of flexible blank holders enabled by finite element analysis

In the stamping process, it is difficult to directly observe the flow of blanks in each zone and effectively define the location of the flow rate change in practical forming. To facilitate the implementation, finite element analysis is used to define the location of the large flow rate change, and boundaries of the flow rate in the same area are reasonably defined. The nodes in the flange are generated naturally after the mesh is completed, as shown in Fig. 6.

The integral blank holder model is imported into a finite element analysis (FEA) platform, and the optimal constant BHF is identified and applied to obtain the flow rate data of the flange as well as metrics of the forming quality, i.e., the maximum thickening ratio, maximum thinning ratio, thickness variation, and equivalent plastic strain (see Table 8 in Appendix 1). The flow rate of nodes selected according to "Circumferential segmentation of a blank holder" section can be identified and illustrated to find the segmentation nodes in each defined height. With segmentation nodes in all heights, the optimal circumferentially segmented scheme and the corresponding FEA model are obtained.

After obtaining the circumferential segmentation model, it is imported into the FEA platform, and the circumferential segmentation model is loaded with the optimal constant BHF. Note that the optimal BHF acting on each circumferential segmentation can be identified by processing and optimization. The flow rate of nodes selected according to "Segmentation of distributed blank holder based on flow rate" section can be identified to find the segmentation nodes in each defined height. The radially segmented scheme and the corresponding FEA model are obtained with segmentation nodes at all heights. The distributed scheme with the circumferentially and radially segmented holding can be finally created, and the metrics obtained are used to validate and modify the segmented holding.

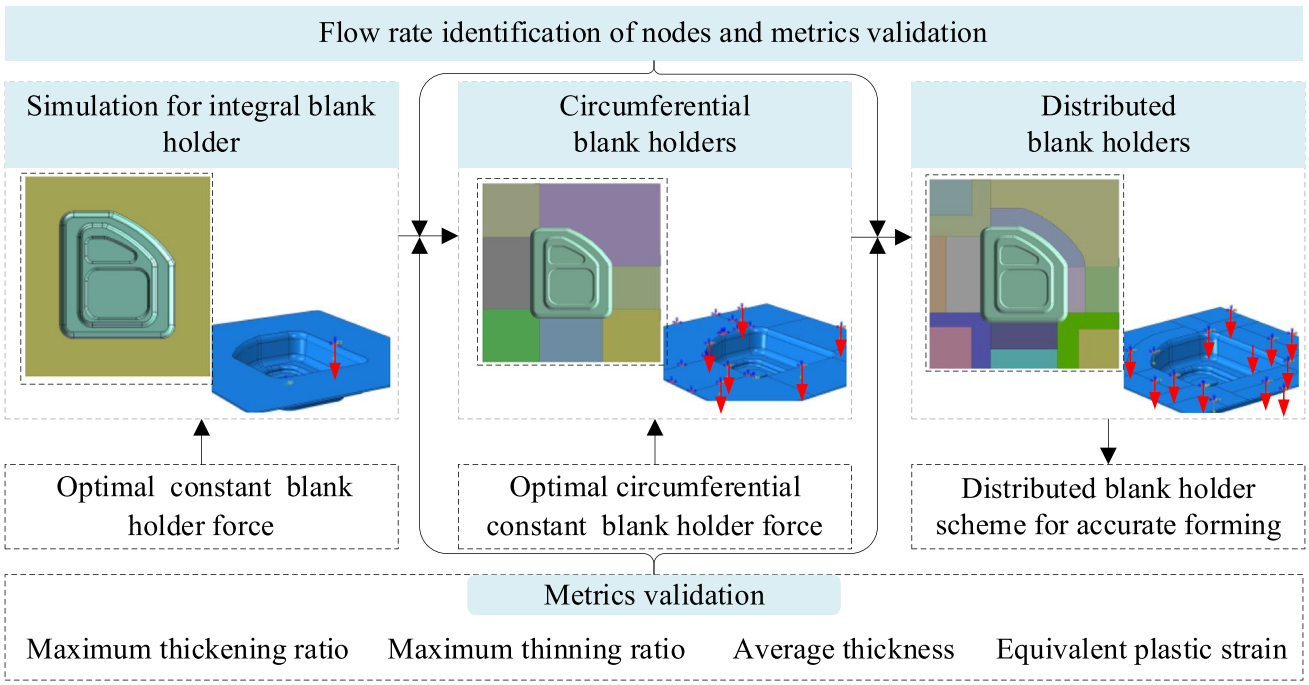

Fig. 6 Implementation of the segmented approach in simulation

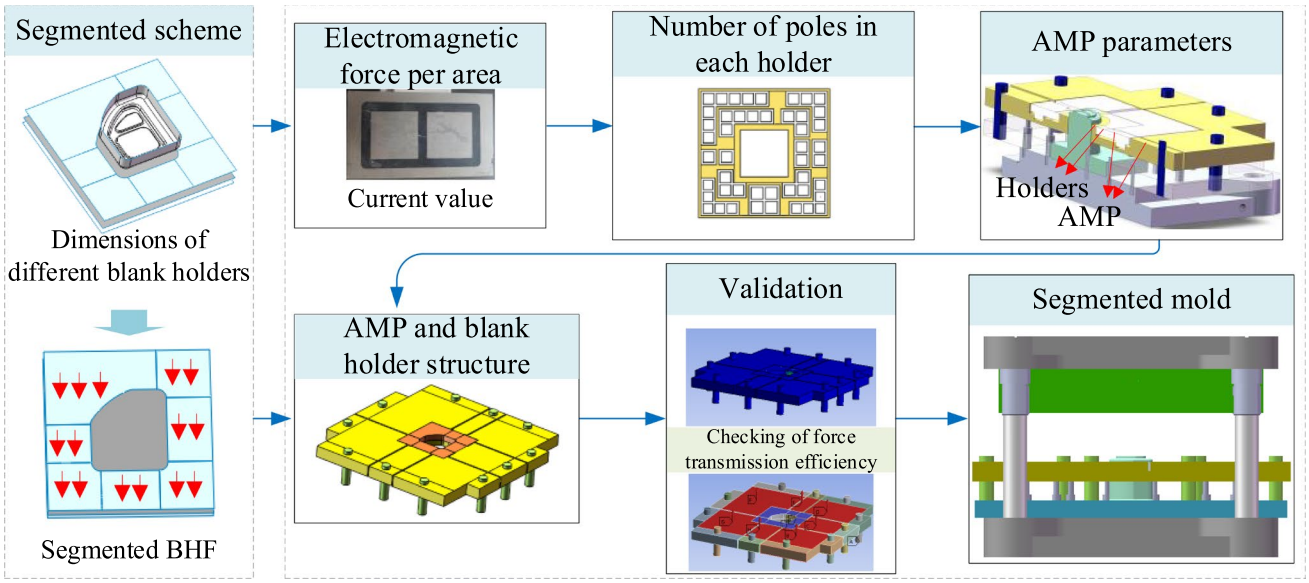

Fig. 7 Flow to design the electromagnetic transmission for segmented blank holding

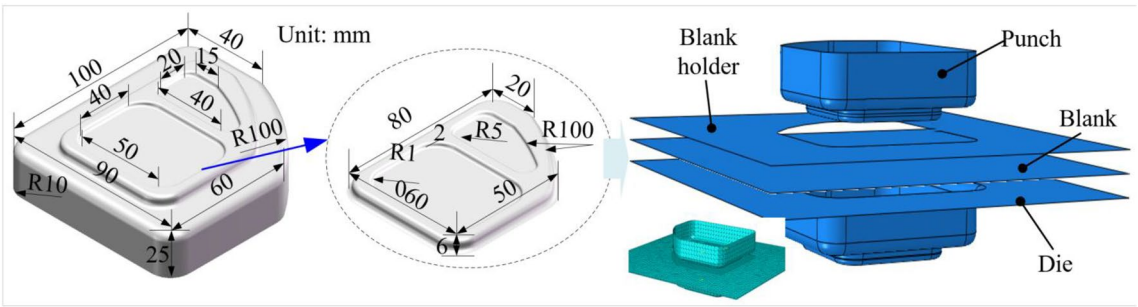

Fig. 8 Profiles of the downscaling part of the car door

With the determined distributed scheme for blank holders, the blank holding system driven by electromagnetics can be subsequently designed, as shown in Fig. 7. According to the maximum electromagnetic force of each pole and obtained optimal segmented BHF, the number of poles required for each holder can be determined. Given the individual pole area, the minimum area of the AMP for each holder can be determined. To reduce the interaction between the magnetic poles, AMPs need to be reasonably distributed to determine the area of AMP as well as the location and number of poles.

The structure and connection of the blank holder and the amplification plate are designed to ensure the expected function is completed, i.e., moving with the EPM. After completing the design, the strength check and force transfer efficiency are verified and modified for holding force. With the determined electromagnetic device, blank holder, and amplification plates, the structural design of the die and punch is carried out, and the overall design of the die is finally completed.

Results and discussions

To validate the feasibility of the flow rate-based segmentation design, a downscaling part of a car door is selected to carry out distributed blank holder schemes, as shown in Fig. 8.

Table 1 Property of the used material DP600 performance parameter

Density (kg/m^3)	Poisson's ratio	Elastic modulus (GPa)
7.85	0.28	207

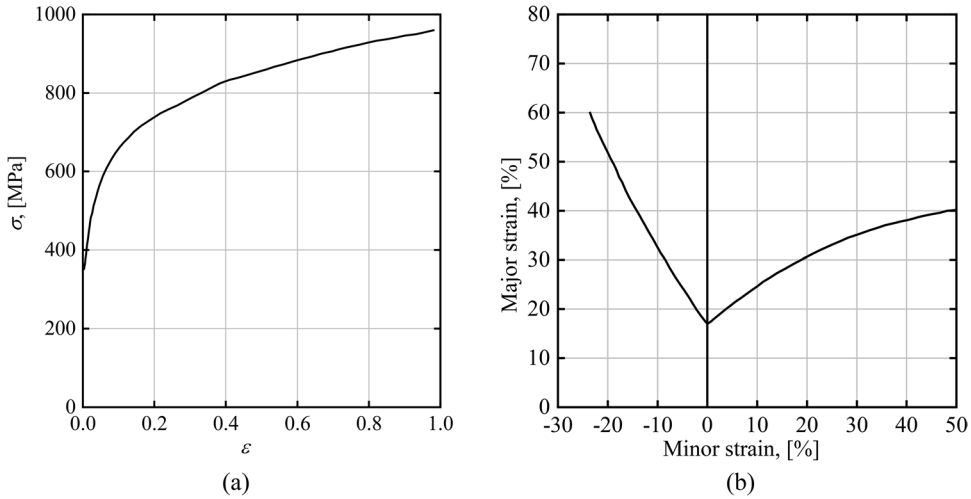

Fig. 9 Stress–strain curve and forming limit of DP 600 employed in the FEA simulation: (**a**) Stress–strain curve, and (**b**) FLC [28]

The operating flow is implemented, and the optimal BHF is given in the FEA simulation platform i.e., ABAQUS. Note that the material used in FEA is DP600, the related properties are shown in Table 1, and the stress–strain curve and FLC curve are tabulated in Fig. 9. The thickness of the blank is 1 mm, and the size of the blank is 180 mm × 180 mm, and the mesh size is 2 mm × 2 mm.

Segmented for distributed blank holder based on simulation

The integral blank holder model is imported into a finite element analysis (FEA) platform, the optimal BHF loaded on the holder is 50 kN, and the thickness variations and equivalent plastic strain diagram of the downscaling part of the car door are shown in Fig. 10.

As seen in Fig. 10, the maximum thickness of the stamped part is located at the edge of the straight area, and the thinnest thickness is located at the round corner. Usually, wrinkling instability occurs with a thickening ratio larger than 20%, and rupture instability occurs when the thinning ratio reaches larger than 30% [29]. The deformation area has a thickening ratio of 16.53%, close to the critical instability value. The possibility of wrinkling instability is great, and it is needed to increase the BHF. By contrast, the maximum thinning ratio is 21.50% in the deformation area at the corner, which is close to the rupture instability value, and the BHF needs to be reduced.

Three sets of closed-loop nodes along the features of the part at relative equivalent radius distances on the blank holder, i.e., l_1, l_2, and l_3, are selected to determine the location of the circumferential segmentation line based on the rates of the selected nodes. The distance between two adjacent lines is 10 mm. The flow rates of all nodes in the three lines are identified at each height and collected every 1.25 mm downstream till the part is stamped. The numbers of the segmentation nodes are recorded, and related nodes are connected. The intersections of all connection locations are

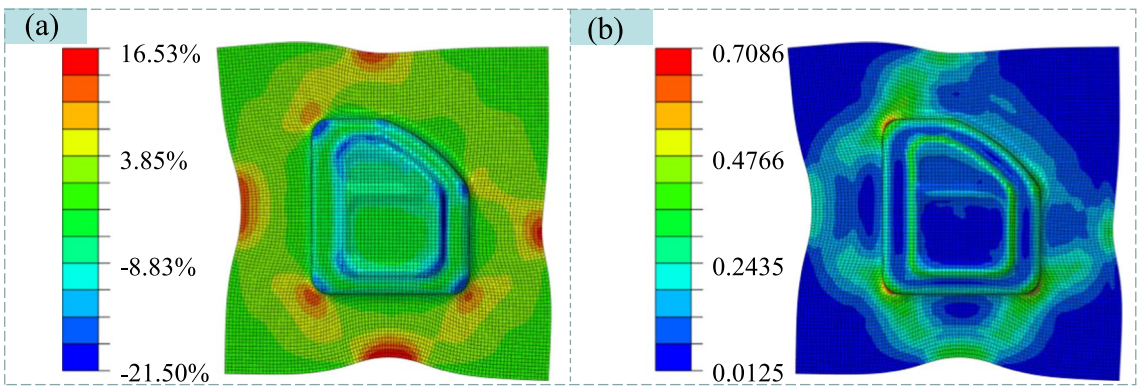

Fig. 10 Forming quality of the part stamped by the integral blank holder: (**a**) Thickness variations and (**b**) Equivalent plastic strain diagram

processed according to "Circumferential segmentation of a blank holder" and "Implementation of flexible blank holders enabled by finite element analysis" sections to form the circumferentially segmented boundaries.

For the ratio of change, if q is too large, large shear stress will occur; otherwise, more segmented holders will be needed. q is set to 25% in this paper, i.e., when the ratio of change of rate value between two adjacent nodes is greater than or equal to 25%, the neighboring nodes can be used for segmentation. The connections of the nodes when the depth is 8.75 mm, and 18.75 mm are used, and the circumferentially segmented scheme of the blank holder is determined, as shown in Fig. 11. The corresponding flow rates of all nodes in three lines are provided in Fig. 21 in Appendix 2.

It is determined that the reasonable BHF of the door parts under the overall blank holder loading is 50.25 kN. The BHF of each segment for each blank holder is shown in Table 2. Note that HC1 to HC7 are the identified circumferential segments.

Using the circumferentially segmented blank holder and loading the optimal BHF for simulation, the maximum thickening ratio, the maximum thinning ratio, and the equivalent plastic strain can be obtained, as shown in Fig. 12. The maximum thickening ratio is 16.59%, and the maximum thinning ratio is 19.45%, and the maximum *peeq* is 0.7696. Compared to the results shown in Fig. 10, the forming quality is improved.

Table 2 Blank holding force for each circumferential segment

Holder	Force/kN	Total/kN
HC1	5.63	50.25
HC2	11.25	
HC3	5.63	
HC4	7.50	
HC5	4.00	
HC6	12.19	
HC7	4.06	

Different node sets l_a to l_g are selected in different circumferential areas to determine the radial segmentation line location. The flow rates of all nodes in the seven lines are identified, and the node data is collected every 1.25 mm downstream till the part is stamped. Nodes with mutations in the rate of selected frames and nodes with significant changes in the rate interval are depicted in the coordinate diagram. The numbers of the segmentation

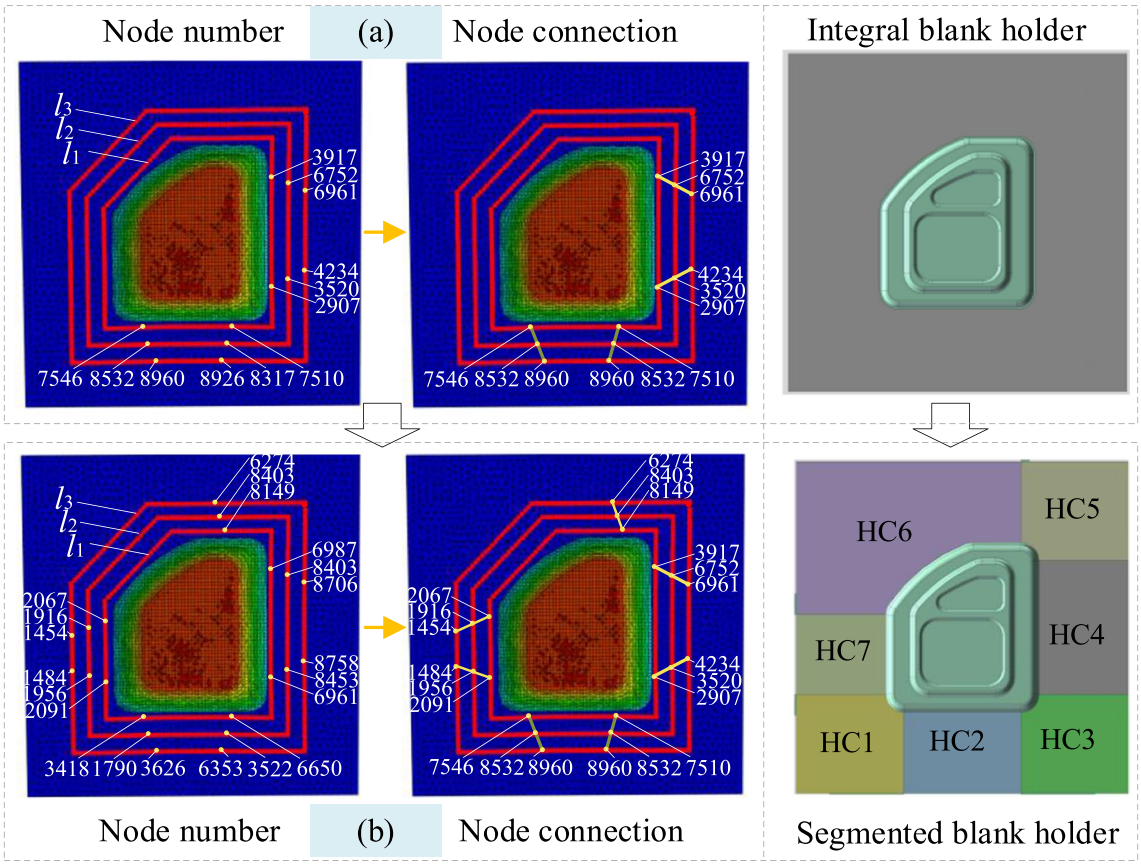

Fig. 11 Node and its number with flow rate for circumferentially segmented blank holder: (**a**) The stamping depth is 8.75 mm and (**b**) The stamping depth is 18.75 mm

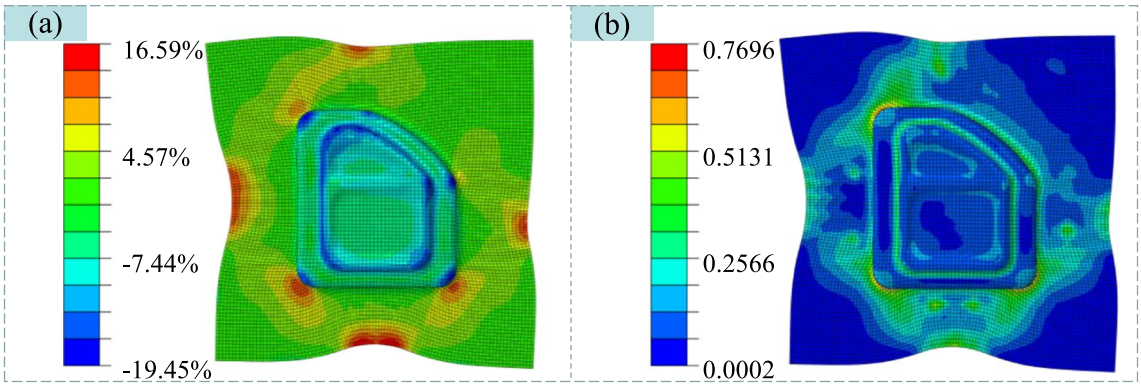

Fig. 12 Thickness variations and equivalent plastic strain of circumferential partition: (**a**) Thickness variations and (**b**) Equivalent plastic strain diagram

nodes at each height are recorded, and related nodes are connected. The intersections of all connection locations are processed according to "Segmentation of distributed blank holder based on flow rate" and "Implementation of flexible blank holders enabled by finite element analysis" section to form the radially segmented boundaries, and the distributed scheme is determined. The connections of nodes when the depth is 8.75 mm, and 18.75 mm are illustrated, as shown in Fig. 12. The corresponding flow rates of all nodes in seven lines are provided in Fig. 22 in Appendix 2.

According to the locations of the corresponding segmentation nodes shown in Fig. 13, the segmentation lines can be determined, and the intersection of the lines is taken to determine the distributed boundaries for the distributed blank holder. The value of the optimal BHF is identified, as shown in Table 3.

The optimal BHF values of the distributed blank holder are brought into the simulation model, and the forming qualities are obtained, as shown in Fig. 14.

The forming metrics are simulated with distributed blank holders, circumferential holders, and integral holders, as

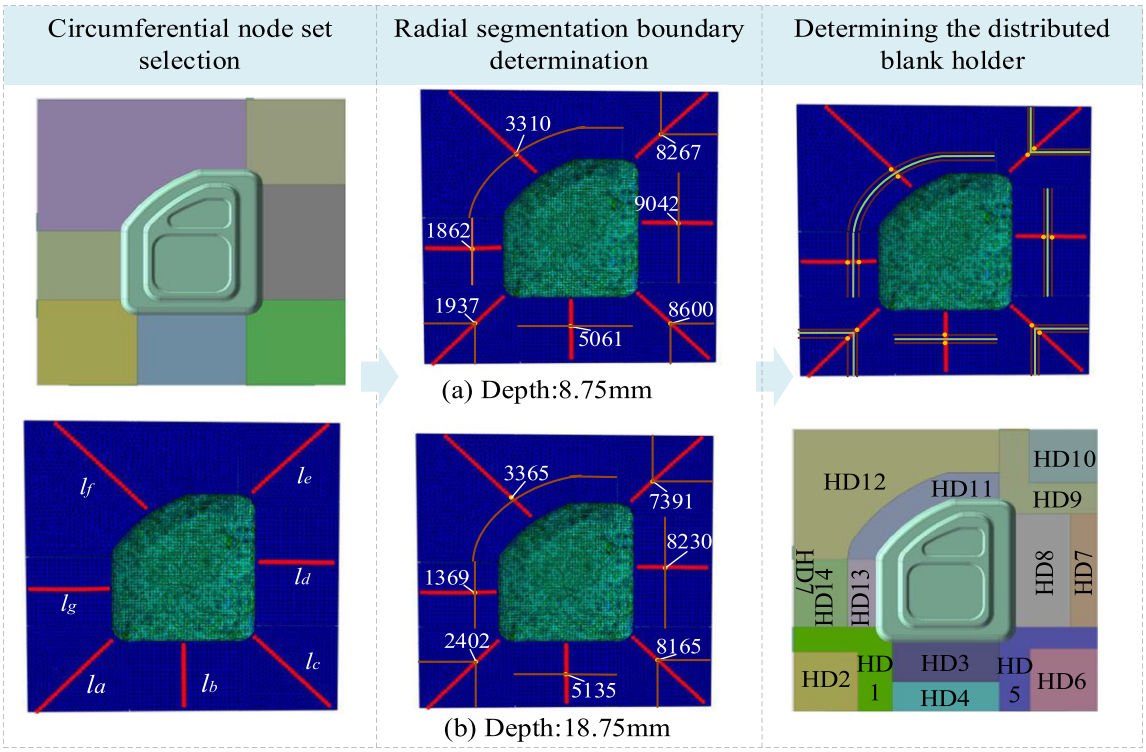

Fig. 13 Node and its number with flow rate for the radially segmented blank holder. (**a**) The stamping depth is 8.75 mm, (**b**) The stamping depth is 18.75 mm

Table 3 Blank holding force for each distributed segment

Holder	Force/kN	Total/kN
HD1	2.00	48.90
HD2	2.20	
HD3	3.50	
HD4	4.00	
HD5	2.75	
HD6	4.40	
HD7	4.38	
HD8	3.12	
HD9	1.80	
HD10	2.00	
HD11	3.81	
HD12	10.87	
HD13	2.19	
HD14	1.88	

shown in Table 4. Results show that the maximum thickening ratio of the distributed blank holder stamped parts is 0.60% and 0.54% higher than the integral and segmented blank holder stamped parts, respectively. The maximum thinning ratio was reduced by 3.90% and 1.85%. The equivalent plastic strain was reduced by 3.23% and 10.90%. It indicates that the flow rate-based design distributed blank holder can significantly improve the forming quality of the stamped parts, make the blank fully stretched, and reduce the risk of damage.

Prototype of the segmented holding system driven by electromagnetics

Since the forming qualities of the parts stamped by circumferential and distributed segmented holders are similar in this case, the circumferential one was designed based on the electromagnetic segmentation holding system in "Segmented blank holding system driven by electromagnetics" section. The structure of the circumferentially segmented dies is easy to control, and the segmented and integral dies were configured based on the identified scheme in "Segmented for distributed blank holder basedon simulation" section and the design flow in "Implementation of flexible blank holders enabled by finite element analysis" section. The structure comprises a die, punch, circumferentially segmented blank holder, amplification plate, electronically controlled permanent magnetic, and gas spring, as shown in Fig. 15.

When using the designed die for forming, the overall and circumferentially segmented dies are fixed to the hydraulic press, and the upper die base of the die is driven by the lifting of the working platform of the hydraulic press to complete the stamping work. A hydraulic press provides the punching force, and a multi-channel power source loads the electronically controlled permanent magnetic current. The electromagnetic force is generated by the loading current through the power supply, which is then transformed into the BHF through the amplification plate to ensure the operation of the press (See Fig. 23 in Appendix 3). Different locations of blank holders correspond to varying numbers of pole pieces. The maximum electromagnetic force generated by each pole piece is 1000N.

Effect of the distributed holder on forming quality

The DP600 was used as the experimental blank, and the stamping experiment was carried out using an integral blank

Table 4 Comparison of the integral and circumferential partitioning and distributed blank holder indicators

Types of the blank holder	α_{max}	β_{max}	γ	$peeq$
Integral holder	16.53%	21.50%	4.43%	0.7086
Circumferentially segmented holder	16.59%	19.45%	4.50%	0.7696
Distributed holder	17.13%	17.60%	4.35%	0.6857

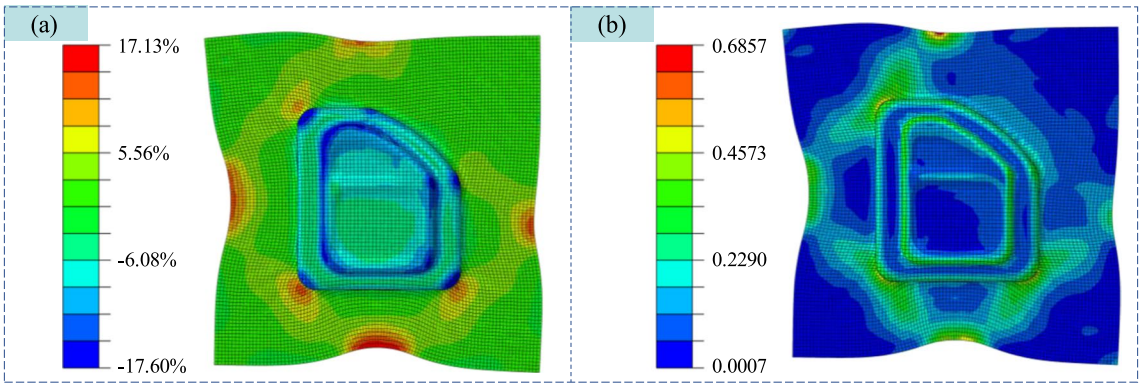

Fig. 14 Forming quality of the part stamped by the distributed blank holder: (**a**) Thickness variations and (**b**) Equivalent plastic strain diagram

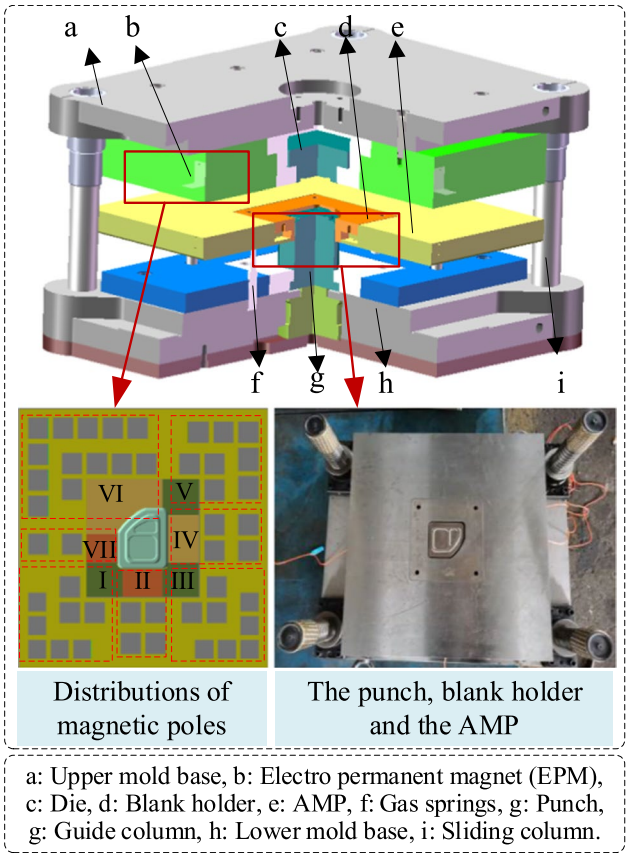

Fig. 15 Prototype of the developed dies of the circumferentially segmented blank holder and the conventional integrated one driven by electromagnetics

holder die and a segmented blank holder die. Firstly, the integral blank holder die is used, and the best quality stamping parts were obtained by adjusting the magnitude of the EPM current value. Giving the EPM a loading current of 40A for different holding areas, the stamped parts of a car door's optimally reduced downscaling part were obtained, as shown in Fig. 16(a). Secondly, with other conditions remaining unchanged, the current values for the holding area loaded are shown in Table 5. The optimal stamped part of the partitioned blank holder is obtained, as shown in Fig. 16(b). The quality metrics of the two types of stamped parts were compared, including the maximum thickening ratio, the maximum thinning ratio, and the average thickness of the parts.

The thickness gauge is used to measure the thickness of the stamped part according to the location of easy thinning or thickening in the simulation results, as shown in Fig. 16(c), and the thickness values at different locations are tabulated in Table 6.

The comparison of the thickness values at different locations shows that the thickening ratio is reduced by 15.4% and 31.7% at locations 1 and 2, and the thinning ratio is reduced by 22.5%, 33.2%, and 36.9% at locations 3, 4, and 5. The experimental results show that using the segmented blank holder can significantly improve the thickness value of the stamped parts and enhance the forming quality.

We selected the downscaled car door part for our study due to its multiple forming features, which closely resemble an actual automotive door (see Fig. 8). This similarity allows us to observe the strain and flow rate evolution during deformation, making our proposed segmentation method feasible

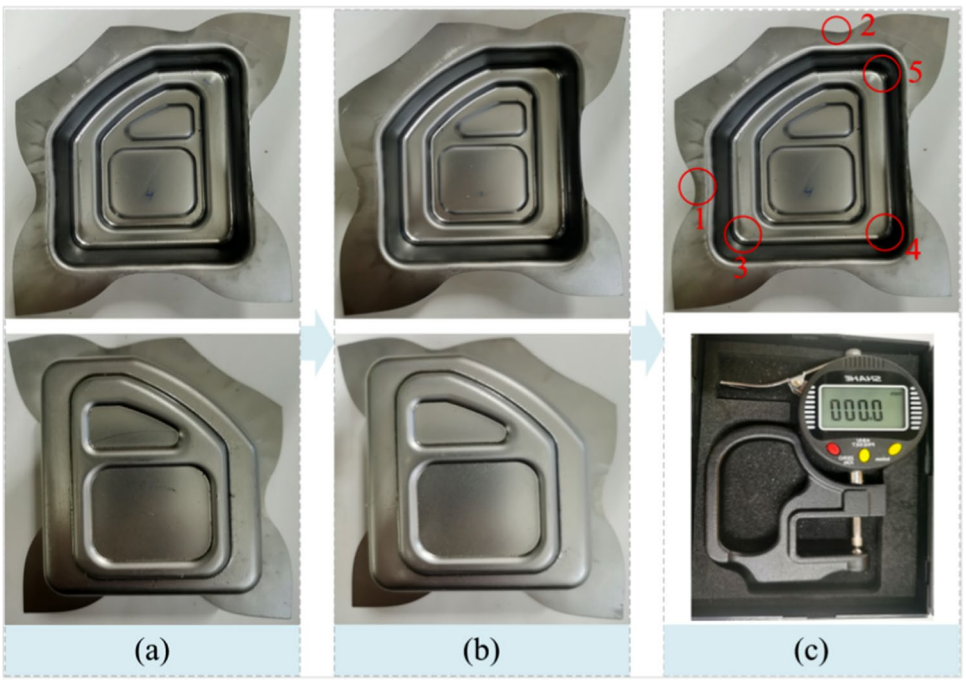

Fig. 16 Stamped parts and thickness measurement: (**a**) Formed by the integral blank holder, (**b**) Formed by the circumferential segmented blank holder, and (**c**) Measurement locations

Table 5 Current values for different holding areas

Holder	HC1	HC2	HC3	HC4	HC5	HC6	HC7
Current (A)	30 A	45 A	30 A	45 A	30 A	45 A	40 A

Table 6 Thickness comparison between parts stamped by the integral and segmented dies

Part stamped by the integral die			Part stamped by the segmented die			Reduced Ratio (%)
Location	Thickness (mm)	Thickening/ Thinning Ratio (%)	Location	Thickness (mm)	Thickening/ Thinning Ratio (%)	
1	1.123	12.3	1	1.104	10.4	15.4%
2	1.145	14.5	2	1.099	9.9	31.7%
3	0.769	−23.1	3	0.821	−17.9	22.5%
4	0.816	−18.4	4	0.877	−12.3	33.2%
5	0.802	−19.8	5	0.875	−12.5	36.9%

to practical formed parts, as the strain evolution remains consistent across different materials.

However, challenges arise when scaling up to the actual part, as each area's required blank holder force increases sharply. To provide sufficient force, the size of the electromagnetic device generating this force must also increase, leading to an enlarged die size—an issue in applications with limited space. Therefore, it is crucial to develop methods and devices that can generate higher electromagnetic force per unit area under these conditions, which will be the focus of our future research.

Comparison with the conventional segmentation scheme

When radially segmenting the circumferentially segmented blank holder, the radial segmentation boundary of the blank holder at the round corner differs from that in the design provided in "Segmentation of distributed blank holder based on flow rate" section. The radial segmentation line, which is perpendicular to the radial center line (see Fig. 5), is changed to a line perpendicular to the edge of the flange (see Fig. 13). The reason is that the flow rate in this area is different from that in the straight area. It is not only changed along the radial center line, but also varies along the perpendicular direction (see Fig. 3).

To supplement this approach, the segmentation boundary in the area with a complex rheological process, such as the round corner, should be determined by considering the flow rate of more nodes. In this condition, the segmentation could be aligned with the real flow rate change in this area. From the results obtained by simulation (see Table 4) and experiments (see Table 6), it is obvious that the flow rate-based segmented blank holder achieves better-forming quality compared with the integral-based segmented blank holder. In this section, the forming quality is compared with the segmented blank holder inspired by previous research on the box-shaped part, i.e., segmented based on the geometries of the part, as shown in Fig. 17. In the downscaling part of the car door, there are eight different lines along the outline, i.e., four straight lines and four round conner lines, and the blank holder is segmented eight pieces.

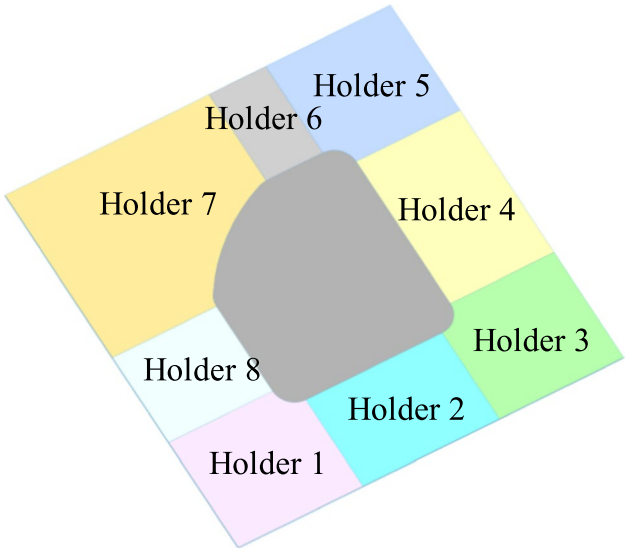

Fig. 17 Conventional segmented blank holder based on the geometries of the part

The blank holder model shown in Fig. 17 was subjected to finite element simulation with all material parameters, boundary conditions, and loading BHF identical to those of the circumferentially segmented blank holder. The quality of the formed part is shown in Fig. 18.

The results and comparison of the two segmentation approaches are shown in Table 7.

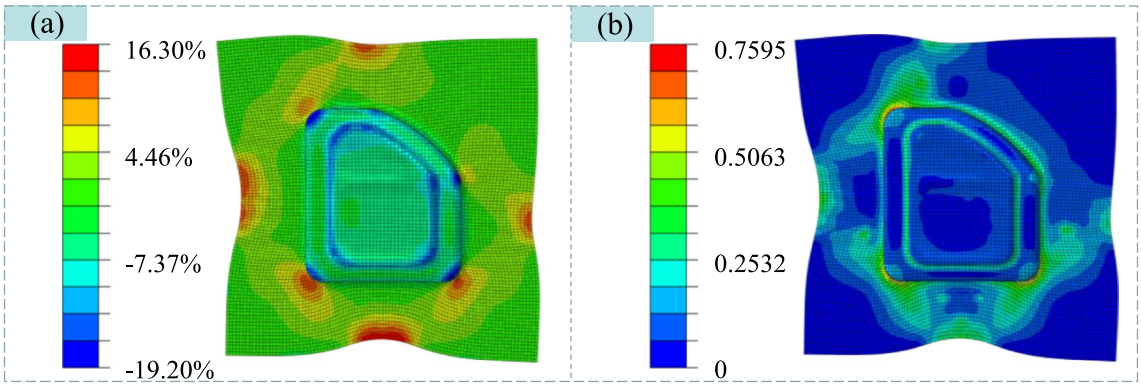

Fig. 18 Forming quality of segmented blank holder based on geometries of the part: (**a**) Thickness variations and (**b**) Equivalent plastic strain diagram

Table 7 Quality comparison of different segmentation approach

Segmentation of blank holder based on geometries		Segmentation of blank holder based on flow rate	
Quality metric	Result Value (%)	Quality metric	Result Value (%)
α_{max}	16.30	α_{max}	16.59
β_{max}	19.20	β_{max}	19.45
peeq	0.7595	*peeq*	0.7696

Compared with the conventional segmentation approach, the maximum thickening ratio is increased by 0.29%, the maximum thinning ratio is increased by 0.25%, and the equivalent plastic strain is increased by 1.33% in the flow rate-based segmentation approach. In comparison, the number of holders in this approach is only seven pieces and decreased by 12.5%. Results show that the flow rate-based approach is close to the conventional approach. The proposed approach reduces the number of blank holders and increases the quality of formed parts. There are only eight lines along the geometries of the downscaling part, and the effects of the reduction of the number of blank holders will be promising with the increase of the complexity of the part.

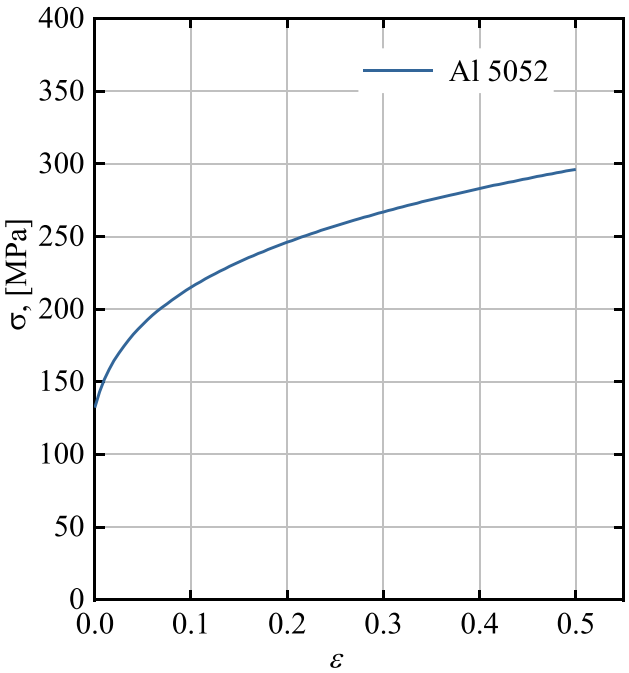

Fig. 19 Stress–strain curve of Al 5052 for validating material's independence

Discussion on the independence of material

To further validate the effectiveness of the flow rate-based segmentation, we changed the material to Al 5052 for forming, and the material's stress–strain is illustrated in Fig. 19. Note that the shape and depth of the stamped parts remained unchanged, to conduct the simulation.

Utilizing our approach, we identified changes and segmented them based on the flow rate at a depth of 13.6 mm, as shown in Fig. 20(a). Then, the distributions of flow rates at four subsequent depths, i.e., 16.8 mm. 20 mm, 22.4 mm, and 24 mm were identified. It was observed that the boundaries with significant rate differences were all located at the edges of the segments, indicating excellent identification performance. Combining with the experiments, and analysis, it is demonstrated that the approach is independent of material. This means that flow rate-based segmentation suits various materials to shape a certain shape. However, the results reveal that the circumferential boundary identification is effective, while the radial segmentation boundaries are not as distinct. Future research will focus on introducing new variables to assist in the precision of radial segmentation.

On the other hand, compared to the traditionally widely used hydraulic cushion technology in industrial applications,

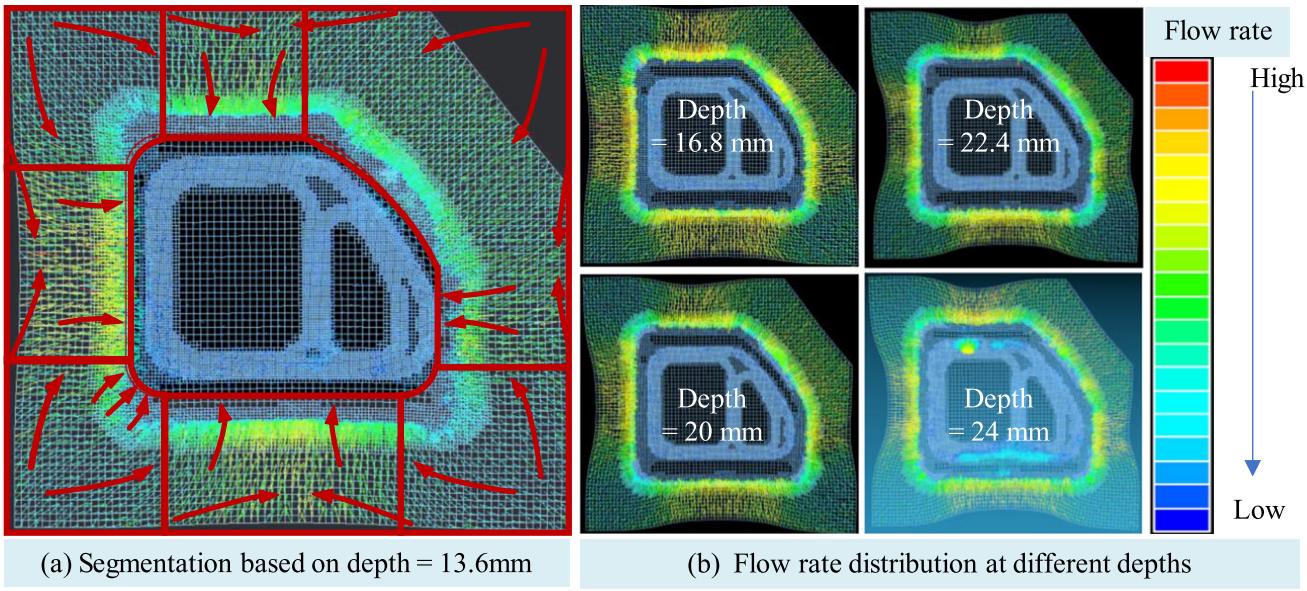

Fig. 20 Segmentation and flow rate distributions in different drawing depths of Al 5052. (**a**) Segmentation of the flange when the depth reaches 13.6 mm, (**b**) Flow rate distributions in different depths, i.e., 16.8mm, 20mm, 22.2mm, and 24mm

the electromagnetic blank holder discussed in this paper may not necessarily result in increased costs. The hydraulic cushion system, which includes components such as accumulators, valves, and hydraulic cylinders, is inherently expensive. While the proposed flow rate-based segmented approach increases the number of independent blank holders, leading to additional processing and control costs, it also offers significant advantages.

This method and configuration are particularly suited for high-precision forming scenarios, such as manufacturing multi-featured panels in the automotive and aerospace industries, where the most substantial benefits will be realized. Moreover, in practical applications, the number of individual blank holders can be reduced by merging adjacent ones based on the required forming precision, thereby achieving a positive cost–benefit balance.

Conclusions

To enable the deformation control of the flexibly segmented blank holding system driven by electromagnetics for complex parts, a flow rate-based design approach considering the flow differences among the flange to segment the blank holder was proposed. The procedures to implement the design were also provided using FEA, and the approach was applied to a downscaling part of the car door. The circumferentially and radially segmented scheme was identified, and the corresponding prototype was developed to validate the feasibility and forming effect. This research laid a foundation for subsequent processes of high-quality stamping. The core contributions are summarized as follows:

(1) Results show that compared with the integral blank holder stamped parts, the maximum thinning ratio was reduced by 3.9%, and the equivalent plastic strain was decreased by 10.9%. It can be concluded that the approach proposed can control the uniformity of the blank flow rate.
(2) The prototype of the electromagnetic segmented holding system was designed to effectively convert electromagnetic force into blank holding force. The structure and working principle of the system were described and applied to the downscaling part of the car door segmentation stamping die, which reduces the occurrence of wrinkle defects. The thickening ratio is reduced by 15.4%, and the thinning ratio is reduced by 22.5%. The developed holding system can flexibly control the segmented BHF to overcome the disadvantages of conventional holding.
(3) The approach can simplify the segmentation of parts with complex geometries compared with conventional geometries-based segmentation. Only seven segmented holders were identified in this case, and this number was reduced by 12.5% compared with that designed by geometries-based segmentation. The die with fewer segmented holders can achieve better forming quality, and the segmentation approach is promising to improve the forming quality of complex parts.

Appendix 1 – Metrics to identify the forming quality of the part

Table 8 Metrics to identify the forming quality of the part

Maximum thickening ratio	Maximum thinning ratio	Thickness variation	Equivalent plastic strain
$\alpha_{max}=\frac{t_{max}-t_0}{t_0}\times 100\%$	$\beta_{max}=\frac{t_0-t_{min}}{t_0}\times 100\%$	$\gamma=\frac{\left(\Sigma_{i=1}^{n}\frac{\lvert t_i-t_0\rvert}{t_0}\right)}{n}\times 100\%$	$peeq=\sqrt{\frac{2}{3}PE^2}$

In this table, a_{max} is the maximum thickening ratio, which can be denoted as the ratio between the difference in the maximum thickness and the initial thickness of the forming parts to the initial thickness, t_{max} is the maximum thickness of the part after forming, and t_0 is the initial blank thickness, PE is the plastic strain tensor.

β_{max} is the maximum thinning ratio, which can be denoted as the ratio between the difference in the initial thickness and the minimum thickness of the formed part to the initial thickness, and t_{min} is the minimum thickness of the part after forming. γ is the thickness variation, which refers to the average thickness value of the whole blank after stamping, t_i is the thickness of any node, and n is the number of total nodes.

$peeq$ is the scalar measure of the equivalent plastic strain at each position in the finite element model, and represents the accumulated plastic strain increment during a simulation. High $peeq$ values indicate significant plastic deformation, which leads to failure.

Appendix 2 – Flow rates of different nodes for segmented holding

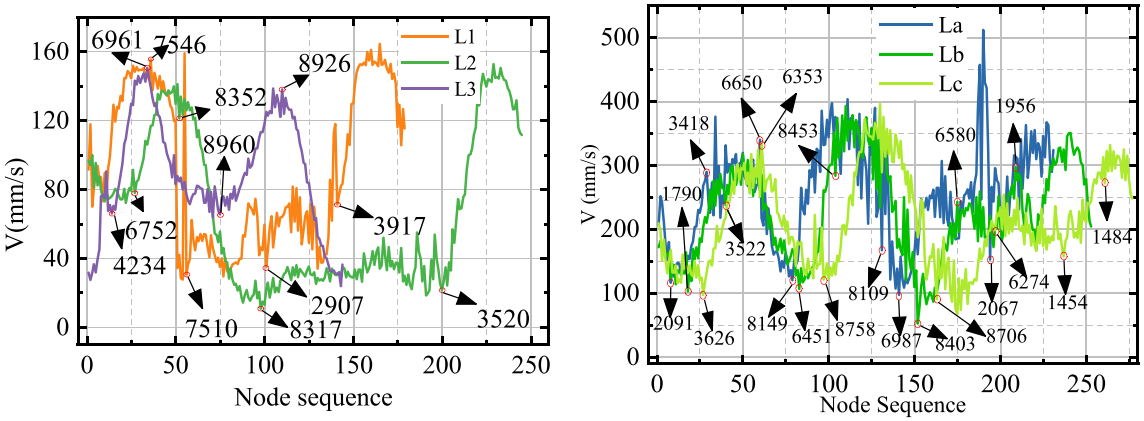

(a) The stamping depth is 8.75 mm

(b) The stamping depth is 18.75 mm

Fig. 21 Flow rates of different nodes for circumferentially segmented holding. (**a**) Flow rates of different nodes when the depth reaches 8.75mm, and (**b**) Flow rates of different nodes when the depth reaches 18.75mm (the value marked is the node number)

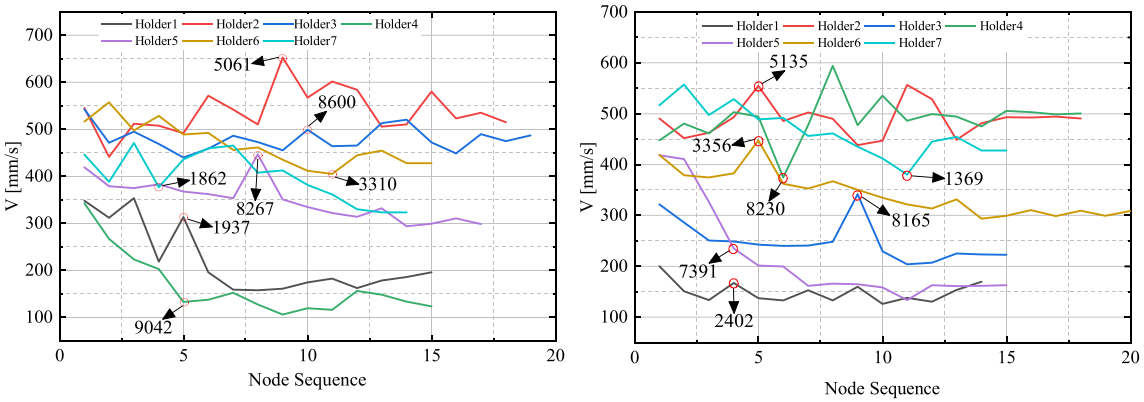

(a) The stamping depth is 8.75 mm (b) The stamping depth is 18.75 mm

Fig. 22 Flow rates of different nodes for distributed segmented holding. (**a**) Flow rates of different nodes when the depth reaches 8.75mm, and (**b**) Flow rates of different nodes when the depth reaches 18.75mm (the value marked is the node number)

Appendix 3 – Configuration of the experimental bench

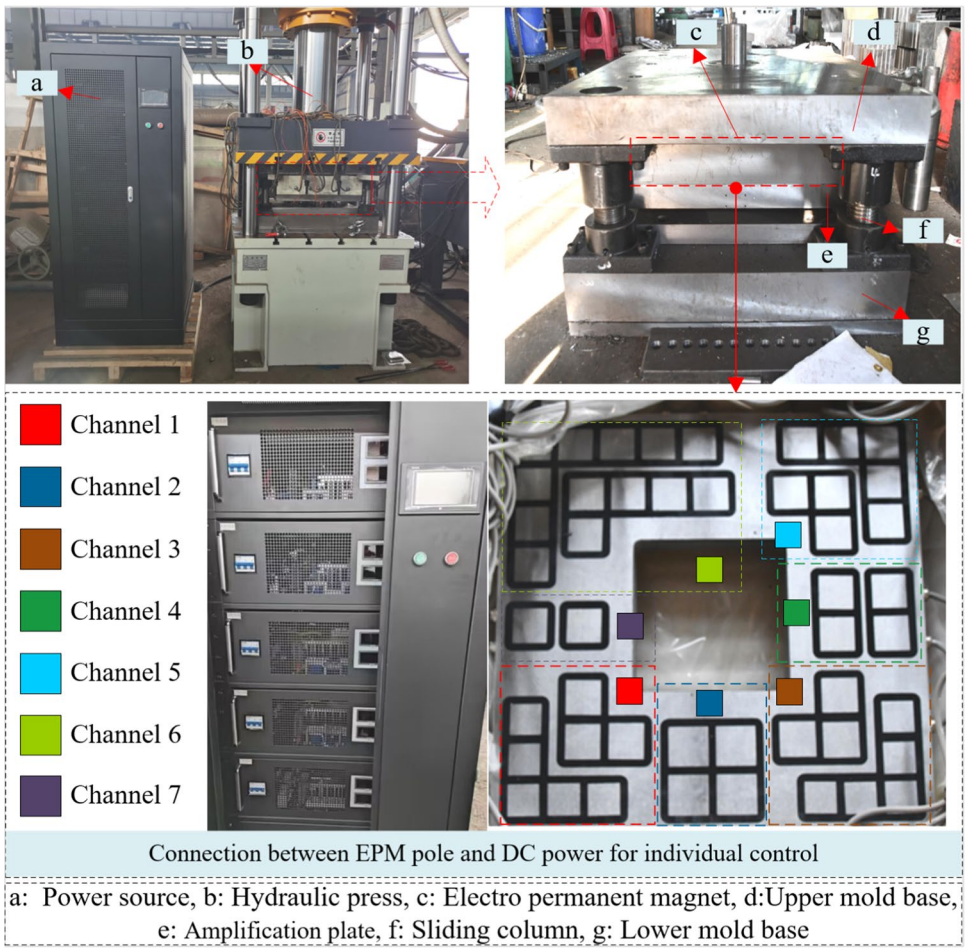

Fig. 23 Configuration of the experimental bench with the configured electromagnetic holding system

Acknowledgements The work is financially supported by the Funds for the National Natural Science Foundation of China under Grant No. U20A20295 and 52005146.

References

1. Kitayama S, Shimizu K, Kawamoto K (2021) Numerical optimization of blank shape and sloped variable blank holder force trajectory for an automotive part. J Adv Mech Des Syst Manuf 15(3):0027
2. Cao J, Banu M (2020) Opportunities and challenges in metal forming for lightweighting: review and future work. J Manuf Sci Eng 142(11):110813
3. Su C, Zhang K, Lou S, Xu T, Wang Q (2017) Effects of variable blank holder forces and a controllable drawbead on the springback of shallow-drawn TA2M titanium alloy boxes. Int J Adv Manuf Technol 93(5):1627–1635
4. Palmieri ME, Lorusso VD, Tricarico L (2021) Robust optimization and kriging metamodeling of deep-drawing process to obtain a regulation curve of blank holder force. Metals 11(2):319
5. Huang H, Lv Q, Li L, Xu Y, Liu C, Zhang T, Liu Z (2023) Individually segmented blank holding system driven by electromagnetics for stamping: Modeling, validation, and prototype. J Mater Process Technol 313:117883
6. Huang H, Sang H, Li L, Wang Y, Zhu L, Liu Z (2023) High-accuracy control of variable blank holding force driven by electromagnetics based on pulse width modulation with grading voltage and mode matching. J Mater Process Technol 322:118210
7. Siegert K, Ziegler M, Wagner S (1997) Closed loop control of the friction force. Deep drawing process. J Mater Process Technol 71(1):126–133
8. Li XN, Liu LX, Wang JP, Jiang CY, Wang ZQ (2011) Influence of segmented blank holder for rectangular box drawing. Adv Mater Res 189–193:2495–2498
9. Tommerup S, Endelt B (2012) Experimental verification of a deep drawing tool system for adaptive blank holder pressure distribution. J Mater Process Technol 212(11):2529–2540
10. Fallahiarezoodar A, Gupta T, Goertemiller C, Altan T (2019) Residual stresses and springback reduction in U-channel drawing of Al5182-O by using a servo press and a servo hydraulic cushion. Prod Eng Res Devel 13(2):219–226
11. Modi B, Kumar DR (2019) Optimization of process parameters to enhance formability of AA 5182 alloy in deep drawing of square cups by hydroforming. J Mech Sci Technol 33(11):5337–5346
12. Srirat J, Yamazaki K, Kitayama S (2012) Optimization of Segmented blank holder shape and its variable blank holder gap in deep-drawing process. J Adv Mech Des Syst Manuf 6(4):420–431
13. Hassan MA, Ahmed KIE, Takakura N (2012) A developed process for deep drawing of metal foil square cups. J Mater Process Technol 212(1):295–307
14. Kitayama S, Koyama H, Kawamoto K, Noda T, Yamamichi K, Miyasaka T (2017) Numerical and experimental case study on simultaneous optimization of blank shape and variable blank holder force trajectory in deep drawing [J]. Struct Multidiscip Optim 55(1):347–359
15. Kitayama S, Koyama H, Kawamoto K, Miyasaka T, Yamamichi K, Noda T (2017) Optimization of blank shape and segmented variable blank holder force trajectories in deep drawing using sequential approximate optimization. Int J Adv Manuf Technol 91(5–8):1809–1821
16. Liu YJ, Li MZ, Ju FF (2017) Research on the process of flexible blank holder in multi-point forming for spherical surface parts. Int J Adv Manuf Technol 89(5–8):2315–2322
17. Tran MT, Shan ZT, Lee HW, Kim DK (2021) Earing reduction by varying blank holding force in deep drawing with deep neural network. Metals 11(3):395
18. Endelt B (2017) Design strategy for optimal iterative learning control applied on a deep drawing process. Int J Adv Manuf Technol 88(1):3–18
19. Seo YR (2008) Electromagnetic blank restrainer in sheet metal forming processes. Int J Mech Sci 50(4):743–751
20. Qin SJ, Yang L, Gai BB (2014) Analysis of wrinkling and rupture in the flange area of axisymmetric deep-drawing forming under planar stress conditions. China Mech Eng 25(23):3221–3226
21. Zhang HS, Qin SJ, Cao LQ, Meng LY, Zhang QR, Li C (2020) Research on deep drawing process using radial segmental blank holder based on electro-permanent magnet technology. J Manuf Process 59:636–648
22. Zhang HS, Qin SJ, Cao LQ (2021) Investigation of the effect of blank holder force distribution on deep drawing using developed blank holder divided into double rings. J Braz Soc Mech Sci Eng 43(6):284
23. Zhang H, Qin S, Meng L (2022) Research on deep drawing with multi-ring blank holder technique. Int J Adv Manuf Technol 122(9–10):4115–4126
24. Chen K, Carter AJ, Korkolis YP (2022) Flange wrinkling in deep-drawing: experiments, simulations and a reduced-order model. J Manuf Mater Process 6(4):76
25. Zhang HS, Qin SJ (2022) A novel process of deep drawing based on electro-permanent magnet combined segmental blank holder technique. Int J Adv Manuf Technol 118(11–12):3883–3896
26. Endelt B, Tommerup S, Danckert J (2013) A novel feedback control system – Controlling the material flow in deep drawing using distributed blank-holder force. J Mater Process Technol 213(1):36–50
27. Emblom WJ (2017) Indirect strain control in aluminum stamp formed pans. J Manuf Sci Eng 139(8):081013
28. Sari SI, Green DE, Vasilescu DM, Song Y (2018) Numerical analysis of damage evolution and formability of DP600 sheet with an extended Rousselier damage model. Int J Solids Struct 134:70–88
29. Jin T, Lei JX, Qiu SH (2010) Optimization of segmented variable holding force liquid-filled drawing process. J Plast Eng 17(04):53–57
30. Jia XD, Zhao CC, He LY, Li JC, Cao MY, Mo C (2017) Analytic methods of flange deformation region in axisymmetrical drawing process. J Mech Eng 53(8):50-57. https://doi.org/10.3901/JME.2017.08.050
31. Li L, Huang HH, Zhao F, Zou X, Mendis G, Luan XN, Liu ZF, Sutherland J (2019) Modeling and analysis of the process energy for cylindrical drawing. J Manuf Sci Eng 141(2):021001. https://doi.org/10.1115/1.4041924